Spatial Periodic Forcing of Turing Structures

Milos Dolnik,* Igal Berenstein, Anatol M. Zhabotinsky, and Irving R. Epstein
Department of Chemistry and Volen Center for Complex Systems, MS 015, Brandeis University, Waltham, Massachusetts 02454-9110
(Received 20 April 2001; published 13 November 2001)

Spontaneously evolving Turing structures in the chlorine dioxide-iodine-malonic acid reaction-diffusion system typically exhibit many defects that break the symmetry of the pattern. Periodic spatial forcing interacts with the Turing structures and modifies the pattern symmetry and wavelength. We investigate the role of the amplitude and wavelength of spatial periodic forcing on the hexagonal pattern of Turing structures. Experimental results and numerical simulations reveal that forcing at wavelengths slightly larger than the natural wavelength of the pattern is most effective in removing defects and producing ordered symmetric hexagonal patterns.

DOI: 10.1103/PhysRevLett.87.238301 PACS numbers: 82.40.Ck, 47.54.+r, 82.40.Bj

Temporal modulation of pattern formation has been studied in a wide variety of systems [1–6], but investigations of spatial modulation of patterns have been largely limited to hydrodynamic behavior in convective fluids [7–11]. Turing structures (TS) [12] arising in reaction-diffusion systems have been investigated in detail under autonomous conditions [13–15] and to some extent with periodic temporal modulation [16–18], but only recently have TS been subjected to spatial modulation. A theoretical study of sidewall periodic forcing of hexagonal TS showed emergence of rhombic patterns [19]. Another theoretical study of TS formation in heterogeneous media suggested that interactions with externally controlled wavelengths and symmetries can give rise to new types of spatiotemporal patterns [20]. An experimental study of Turing-like patterns formed during the polymerization of acrylamide in the methylene blue-sulfide system showed spatial entrainment effects when subjected to spatially periodic perturbation [21].

The chlorite-iodide-malonic acid (CIMA) reaction and its modified version, the chlorine dioxide-iodine-malonic acid (CDIMA) reaction, are the most widely employed reaction-diffusion systems for the study of TS. The photosensitivity of these systems can be used to control and modulate TS. Gunaratne *et al.* [22] used light to initiate regular hexagonal and rhombic patterns in the CIMA reaction. Recently, we have studied in detail the effect of light on the CDIMA reaction and proposed a simple model for its photosensitivity [23]. We also studied the effect of periodic external forcing [17,18] and found resonances in suppression of TS by utilizing spatially uniform, temporally periodic illumination. Here we study external forcing of TS in the CDIMA reaction using temporally constant illumination through a mask consisting of a pattern of hexagons. Modulation of spontaneously formed hexagons is investigated as a function of two parameters—the intensity of illumination and the wavelength of the forcing pattern.

Experiments are carried out in a thermostated continuously fed unstirred reactor (CFUR) at 4.0 ± 0.2 °C. We use a one-sided CFUR, which consists of an agarose (Fluka 05070) gel layer (2% agarose, thickness 0.3 mm, diameter 25 mm) and a single feeding chamber, which is separated from the gel layer by an Anapore membrane (Whatman, pore size 0.2 μm, impregnated with 4% agarose gel) and a nitrocellulose membrane (Whatman, pore size 0.45 μm). The input concentrations of reagents are 0.4 mM I_2, 0.08 mM ClO_2, 10 mM H_2SO_4, 1.2 mM malonic acid, and 2.5 g/L poly(vinyl alcohol) (Aldrich MW 10000). The volume of the feeding chamber is 1.85 ml and the residence time is 230 s. Three magnetic stirrer bars are placed directly under the membranes to maintain homogeneity of the solution in contact with the gel.

The gel layer is illuminated from above by parallel light from a 300 W quartz halogen lamp. The image of a mask with hexagonal patterns of well-defined wavelength is focused on the gel layer. The light intensity is varied between 7.7 and 38.8 mW/cm^2. We use a Sony CCD videocamera with a Hamamatsu camera controller to record spatiotemporal patterns. Reflected light from the tungsten halogen lamp (intensity 2.0 mW/cm^2) is used for image acquisition. The size of the analyzed area is 10 mm × 10 mm (256 × 256 pixels). We evaluate the cross-correlation coefficient C for a pattern and a mask, defined as

$$C = \frac{\sum_x \sum_y (P_{x,y} - \overline{P})(M_{x,y} - \overline{M})}{\sqrt{\sum_x \sum_y (P_{x,y} - \overline{P})^2 \sum_x \sum_y (M_{x,y} - \overline{M})^2}}, \quad (1)$$

where $P_{x,y}$ ($M_{x,y}$) is a grey level of a pattern (mask) at spatial point x, y and $\bar{P}$ ($\bar{M}$)is the mean grey level. We also utilize two-dimensional Fourier spectra to evaluate the rate of modulation of TS.

Formation of stationary TS typically requires 8 to 12 h after the start of an experiment. We begin illumination of these naturally formed patterns with the lowest actinic light intensity. In preliminary experiments, we monitored the effects of light on the TS and observed that the illuminated patterns are essentially stationary after 20 min. Hence, we illuminate a pattern for 20 min with fixed light

intensity and then take a snapshot of the modulated TS thus obtained. Then the actinic light intensity is increased to the next higher level and the pattern is again illuminated through the same hexagonal mask. This procedure is repeated until the maximum light intensity is reached. Usually, with the highest light intensity used, the mask is well imprinted, and the TS have almost perfect symmetry. To destroy this symmetry, we illuminate the pattern for 5 min with intense uniform light (100 mW/cm^2), which results in suppression of the pattern. Illumination through a mask with a different wavelength is started only after a new stationary pattern is formed.

Spontaneous formation of TS results in patterns that do not possess perfect hexagonal symmetry; they include a large number of penta-hepta defects. The Fourier spectrum of such a pattern consists of a circle rather than individual peaks. In the Fourier spectra evaluation, the zero mode is excluded and the spectrum coefficients are normalized to contain values between 0 and 255. Larger average Fourier amplitudes correspond to more disordered patterns.

When TS are illuminated through a mask of hexagons with a wavelength at least 20% smaller ($\lambda_F/\lambda_P < 0.8$), full synchronization with the external forcing does not occur. The pattern becomes modulated at higher light intensities, when spots from the original TS start to break apart. The modulation is detected by the emergence of six peaks in the Fourier spectrum. If the light intensity is further increased, instead of synchronization with the forcing pattern, we observe suppression of TS.

When the wavelength of the forcing hexagons almost exactly matches the wavelength of the pattern, a different scenario is observed (Fig. 1a). The TS spots rearrange themselves in synchrony with the mask pattern. The synchronization becomes more apparent as the light intensity increases and is seen as a decrease in the amplitude of the Fourier spectrum along the circle and the emergence of six peaks corresponding to the forcing spatial frequency. At higher light intensities, the TS are almost perfectly symmetric and fully synchronized with the forcing pattern (Fig. 1a, last snapshot).

Another type of modulation is observed when the pattern is forced by hexagons with wavelength significantly larger than the pattern wavelength. The forcing leads to an increase in the size of the illuminated white spots (Figs. 1b). The Fourier spectrum already reveals this pattern modulation at low light intensities (Fig. 1b, second snapshot). If there are several spots within a single illuminated area, these spots merge and eventually form one large spot with the shape of the illuminated area. Depending on the forcing wavelength, TS spots outside the illuminated area may merge with the large spots formed by illumination (Fig. 1b, last snapshot) or may reorganize between the large spots. Figures 1c and 1d illustrate and quantify the effect of forcing by light as a histogram of the wave number distribution $P(k)$, averaged over the azimuthal angle [24].

Figure 2 summarizes the experimental results. Cross-correlation coefficients evaluated from patterns quantify

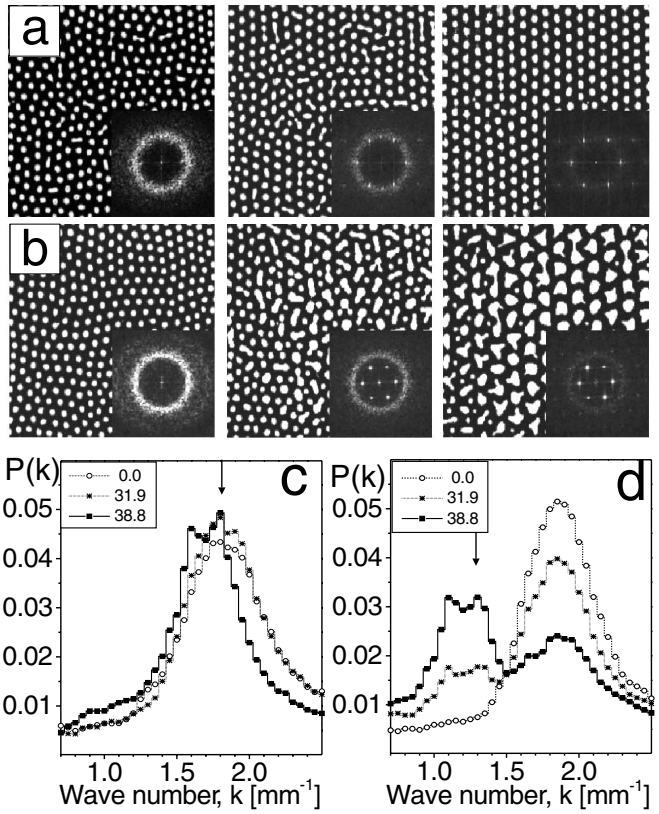

FIG. 1. Modulation of Turing structures with spatial periodic forcing. Average wavelength of natural patterns is $\lambda_P = 0.53$ mm, wavelength of forcing hexagons, λ_F is (a) 0.54 mm and (b) 0.80 mm. First column of snapshots displays patterns before illumination; second and third show patterns modulated by light intensity 31.9 and 38.8 mW/cm^2, respectively. Central parts of 2D Fourier spectra are shown as insets; contrast of Fourier spectra is enhanced to increase visibility of smaller amplitude peaks. Size of pattern snapshots is 10×10 mm; frequency range of displayed Fourier spectra is $\pm 3.2 \times \pm 3.2$ mm^{-1}. (c) and (d) Wave number distributions $P(k)$ averaged over azimuthal angle for patterns shown in (a) and (b). Arrows point to forcing wave numbers; numbers next to symbols specify light intensity in mW/cm^2.

the match between a mask and a pattern. The dip in the region of high correlation occurs at a wavelength ratio λ_F/λ_P between 1.0 and 1.2 (Fig. 2a). The plot also contains maxima of the contour lines for a forcing wavelength about 50% larger than the natural wavelength; for $\lambda_F/\lambda_P \approx 2.0$ the contours display another, very shallow minimum. Figure 2b, which contains contours of average amplitude of the Fourier spectra, displays a similar shape of the contour lines. Additionally, this plot also shows that at some wavelengths the order does not increase monotonically with the forcing amplitude. For example, for $\lambda_F/\lambda_P \approx 1.5$, the average amplitude of the Fourier spectrum first increases slightly with light intensity, and only at higher intensities does this trend reverse. A similar scenario is found for λ_F/λ_P near 1.0 and 2.6.

To compare the experimental results with those of numerical simulations, we employ a two-variable model that includes the effect of illumination [17,23]. The model is

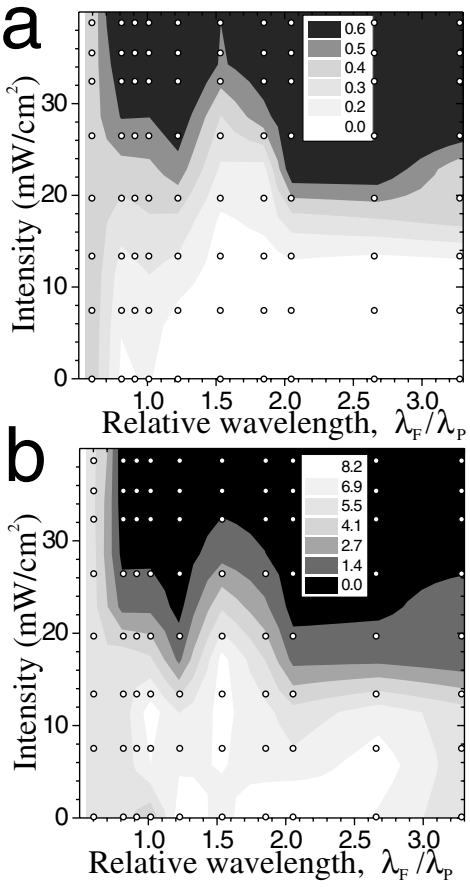

FIG. 2. Dynamics of spatial periodic modulation of Turing structures—experimental results. (a) Contour plot of cross-correlation coefficients evaluated for patterns and mask. (b) Contour plot of average amplitude of normalized 2D Fourier spectra. Grey levels represent values of the coefficients and amplitudes. Open circles represent points at which data are evaluated; contour lines are estimated from interpolation between these points.

$$\frac{\partial u}{\partial t} = a - u - 4\frac{uv}{1+u^2} - w(x,y) + \nabla^2 u,$$
$$\frac{\partial v}{\partial t} = \sigma\left\{b\left[u - \frac{uv}{1+u^2} + w(x,y)\right] + d\nabla^2 v\right\}. \quad (2)$$

Here u and v are the dimensionless concentrations of $[I^-]$ and $[ClO_2^-]$, respectively; a, b, d, and σ are dimensionless parameters. In our simulations, we fix $a = 36$, $b = 2.8$, $d = 1.2$, and $\sigma = 30$, which leads to the formation of hexagonal TS with white spots (low tri-iodide complexing agent concentration) analogous to those obtained in experiments. The rate of the photochemical reaction $w(x, y)$ is a periodic function of the spatial coordinates x and y. A hexagonal array of squares with nonzero values of w was chosen for the simulations. The array of squares can be easily implemented on a rectangular finite difference grid. For integration, we utilize the Euler method with fixed step size 0.001 time units and zero flux boundary conditions. The simulations mimic the experimental changes in the light intensity. As initial conditions, we employ a pattern of TS, prepared by random perturbation of the homogeneous state.

When the forcing wavelength is equal to the pattern wavelength, visible modulation of the TS is seen even for weak forcing ($w = 1$) (Fig. 3a). For $w > 2.0$, the TS are almost perfectly symmetric and fully synchronized with the forcing pattern. As in the experiment, when the forcing wavelength is much larger than the pattern wavelength, forcing first leads to an increase in the size of the illuminated spots and eventually to formation of spots with a shape matching that of the illuminated area (Figs. 3b). For wavelength $\lambda_F \gg \lambda_P$ and intermediate intensity w, "black-eye" patterns are formed [22], which result from resonant interaction between the forcing and intrinsic

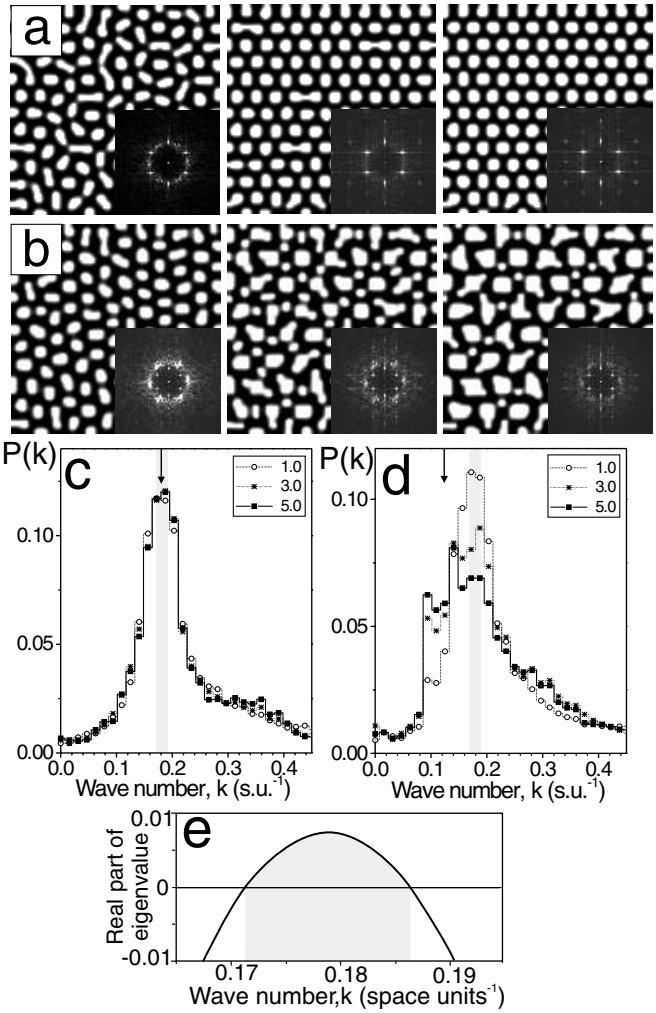

FIG. 3. Numerical simulation of spatial modulation of Turing structures. The number of grid points used is 128 × 128, and the physical length is 64 × 64 dimensionless space units. Relative wavelength λ_F/λ_P is (a) 1.0 and (b) 1.5. First column of snapshots displays modulation for $w = 1$, second for $w = 3$, and third for $w = 5$. Central part of 2D Fourier spectrum is shown as inset. (c) and (d) Wave number distributions $P(k)$ averaged over azimuthal angle for patterns shown in (a) and (b). Arrows indicate wave numbers of the mask. (e) Section of dispersion curve for parameters used in simulations showing range of linearly stable wavelengths.

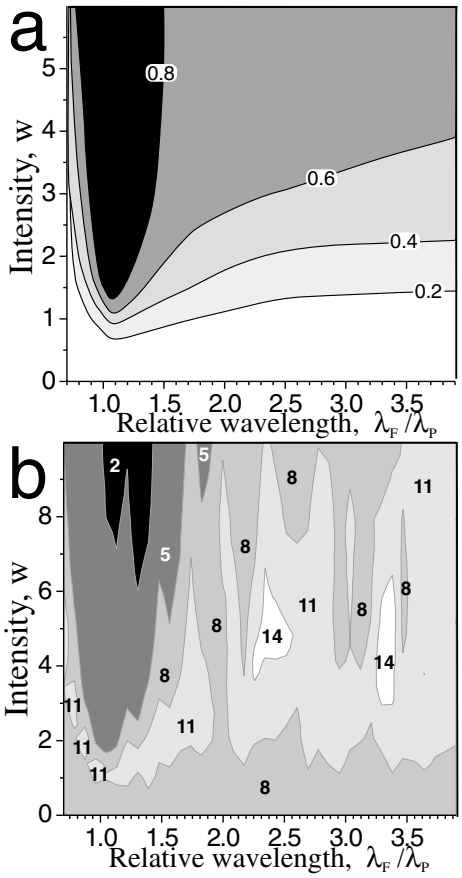

FIG. 4. Analysis of spatial periodic modulation of Turing structures—numerical results. (a) Contour plot of cross-correlation coefficients evaluated for patterns and mask. (b) Contour plot of average amplitude of normalized 2D Fourier spectra. Darker grey levels represent lower values of amplitude; numbers indicate values along grey level boundaries.

pattern wavelengths. Forcing with a wavelength smaller than the natural pattern wavelength results in modulation similar to that observed in the experiments, and full synchronization with the external forcing does not occur. The effect of forcing on the wavelength modulation is further quantified by evaluating the histogram of the wave number distribution $P(k)$, averaged over the azimuthal angle (Figs. 3c and 3d). The range of stable wavelengths obtained from the dispersion curve (Fig. 3e) for the corresponding Turing instability is displayed as grey shading.

The contour lines of the correlation coefficients display minima at λ_F/λ_P between 1.05 and 1.10 (Fig. 4a). As the forcing wavelength is decreased below its "resonant" value, the correlation quickly decays, in good agreement with the experimental results. On the other hand, the "anti-resonant" domain found in the experiments for $\lambda_F/\lambda_P \approx 1.5$ is not seen in Fig. 4a, though it can be detected in Fig. 4b. Figure 4b displays a more pronounced and detailed structure than Fig. 4a. This plot is consistent with the experimental observation that an increase in intensity does not always result in increasing the order of a disordered state.

In this paper, we have studied the modulation of hexagonal TS using hexagonal spatial forcing. Two-dimensional space offers other possibilities for spatial periodic forcing. For example, stripes, rhombs, and squares can be used to study the spatial periodic modulation of TS. Work is currently under way in our laboratory to investigate modulation of TS by other spatially periodic functions. This also includes forcing of striped patterns using striped masks in analogy to experiments performed in nematic liquid crystals with electrohydrodynamic instability [7,8].

This work was supported by the National Science Foundation and the W. M. Keck Foundation.

*To whom correspondence should be addressed.

[1] J. J. Niemela and R. J. Donnelly, Phys. Rev. Lett. **59**, 2431 (1987).
[2] P. C. Hohenberg and J. B. Swift, Phys. Rev. A **35**, 3855 (1987).
[3] M. C. Cross and P. C. Hohenberg, Rev. Mod. Phys. **65**, 851 (1993).
[4] V. Petrov, Q. Ouyang, and H. L. Swinney, Nature (London) **388**, 655 (1997).
[5] A. L. Lin *et al.,* Phys. Rev. Lett. **84**, 4240 (2000).
[6] V. Vanag, A. M. Zhabotinsky, and I. R. Epstein, Phys. Rev. Lett. **86**, 552 (2001).
[7] M. Lowe, J. P. Gollub, and T. C. Lubensky, Phys. Rev. Lett. **51**, 786 (1983).
[8] M. Lowe and J. P. Gollub, Phys. Rev. A **31**, 3893 (1985).
[9] P. Coullet, Phys. Rev. Lett. **56**, 724 (1987).
[10] W. Zimmermann *et al.,* Europhys. Lett. **24**, 217 (1993).
[11] R. Schmitz and W. Zimmermann, Phys. Rev. E **53**, 5993 (1996).
[12] A. M. Turing, Philos. Trans. R. Soc. London B **237**, 37 (1952).
[13] V. Castets *et al.,* Phys. Rev. Lett. **64**, 2953 (1990).
[14] J. Boissonade, E. Dulos, and P. De Kepper, in *Chemical Waves and Patterns,* edited by R. Kapral and K. Showalter (Kluwer, Dordrecht, 1995), p. 221; Q. Ouyang and H. L. Swinney, *ibid.,* p. 269; I. Lengyel and I. R. Epstein, *ibid.,* p. 297; P. Borckmans, G. Dewel, A. De Witt, and D. Walgraef, *ibid.,* p. 323.
[15] R. Rudovics, E. Barillot, P. Davies, E. Dulos, J. Boissonade, and P. De Kepper, J. Phys. Chem. **103**, 1790 (1999).
[16] A. Careta and F. Sagues, J. Chem. Phys. **92**, 1098 (1990).
[17] A. K. Horvath *et al.,* Phys. Rev. Lett. **83**, 2950 (1999).
[18] M. Dolnik, A. M. Zhabotinsky, and I. R. Epstein, Phys. Rev. E **63**, 026101 (2001).
[19] V. Perez-Muñuzuri *et al.,* Physica (Amsterdam) **82D**, 195 (1995).
[20] J. P. Voroney, A. T. Lawniczak, and R. Kapral, Physica (Amsterdam) **99D**, 303 (1996).
[21] F. Fecher *et al.,* Chem. Phys. Lett. **313**, 205 (1999); M. Watzl and A. F. Munster, J. Phys. Chem. A **102**, 2540 (1998).
[22] G. H. Gunaratne, Q. Ouyang, and H. L. Swinney, Phys. Rev. E **50**, 2802 (1994).
[23] A. P. Muñuzuri, M. Dolnik, A. M. Zhabotinsky, and I. R. Epstein, J. Am. Chem. Soc. **121**, 8065 (1999).
[24] M. S. Heutmaker and J. P. Gollub, Phys. Rev. A **35**, 242 (1987).